



# Pyruvate Kinase M2 Nuclear Translocation Regulate Ferroptosis-Associated Acute Lung Injury in Cytokine Storm

Haiting Wang<sup>1,4</sup>, Chenyu Fan<sup>2</sup>, Xuelian Chen<sup>3</sup>, Wei Zhou<sup>2</sup>, Li Guo<sup>1</sup>, Feng Zhao<sup>2</sup>, Shuang Ye<sup>1</sup>, Shuangjun He<sup>2,5</sup> and Yi Chen<sup>2,5</sup>

Received 8 November 2023; accepted 28 February 2024

**Abstract**—Cytokine storm (CS) is linked with macrophage dysfunction and acute lung injury (ALI), which can lead to patient mortality. Glycolysis is preferentially exploited by the pro-inflammatory macrophages, in which pyruvate kinase M2 (PKM2) is a critical enzyme. The mechanism underlying the link between CS and ALI involves cell death, with the recently discovered programmed cell death known as ferroptosis being involved. However, the relationship between the glycolysis and ferroptosis in the context of CS-related ALI remains unclear. CS-associated ALI induced by poly I:C (10 mg/kg, i.v) and LPS (5 mg/kg, i.p) (IC: LPS) exhibit significant ferroptosis. Ferrostatin-1 (ferroptosis inhibitor) treatment attenuated IC:LPS-induced mortality and lung injury. Moreover, Alveolar macrophage (AM) from IC:LPS model exhibited enhanced glycolysis and PKM2 translocation. The administration of ML-265(PKM2 monomer/dimer inhibitor) resulted in the formation of a highly active tetrameric PKM2, leading to improved survival and attenuation of ALI. Furthermore, ML-265 treatment decreased ferroptosis and restored the balance between anaerobic glycolysis and oxidative phosphorylation. Notably, in patients with lung infection, intracellular expression level of PKM2 were correlated with circulating inflammation. Enhanced ferroptosis and PKM2 nuclear translocation was noticed in CD14<sup>+</sup> blood monocytes of lung infection patients with CS. In conclusion, PKM2 is a key regulatory node integrating metabolic reprogramming with intra-nuclear function for the regulation of ferroptosis. Targeting PKM2 could be explored as a potential means in the future to prevent or alleviate hyper-inflammatory state or cytokines storm syndrome with aberrant ferroptotic cell death.

**KEY WORDS:** cytokine storm; acute lung injury; ferroptosis; pyruvate kinase M2

Haiting Wang and Chenyu Fan Authors have contributed equally.

<sup>1</sup>Department of Rheumatology, Renji Hospital, Shanghai Jiao Tong University School of Medicine, Shanghai, China

<sup>2</sup>Department of Emergency and Critical Care Medicine, Renji Hospital, Shanghai Jiao Tong University School of Medicine, Shanghai, China

<sup>3</sup>Department of Burn, Ruijin Hospital, Shanghai Jiao Tong University School of Medicine, Shanghai, China

<sup>4</sup>Department of Immunology and Microbiology, Shanghai Institute of Immunology, Shanghai Jiao Tong University School of Medicine, Shanghai, China

<sup>5</sup>To whom correspondence should be addressed at Department of Emergency and Critical Care Medicine, Renji Hospital, Shanghai Jiao Tong University School of Medicine, Shanghai, China. Email: rjhsj1981@126.com cheniyirenji@126.com

## INTRODUCTION

The cytokine storm (CS), a hyperactivated immune response, is one of the largest current issues worldwide since the advent of the COVID-19 pandemic [1, 2]. It has been linked with acute lung injury (ALI) and multiple organ failure [3]. Innate immune cells are central to the CS pathogenesis because they express a range of pattern recognition receptors, including Toll-like receptors (TLRs), which are activated by endogenous and exogenous inflammatory signals [4]. Murine models of CS have demonstrated that sustained TLR activation is sufficient to amplify proinflammatory cytokine production and induce CS-mediated immunopathology [5]. Similarly, successive Poly I:C (TLR3) and LPS (TLR4) (IC: LPS) activation in wild type mice may induce clinical manifestations of CS, including hepatosplenomegaly, hepatitis, cytopenia, and hypercytokinemia [6]. Patients with CS syndrome exhibit increased numbers of pulmonary inflammatory macrophages, which are also linked to macrophage dysfunction [7], suggesting that macrophages may be a therapeutic target for inhibiting the CS syndrome. Elevated levels of several inflammatory factors are typical features of a CS, which can lead to an unfavorable prognosis [8, 9]. However, blocking pro-inflammatory cytokines such as TNF- $\alpha$ , IL-1, or IL-6 have had inconsistent results in the treatment of the CS syndrome [4, 10], suggesting a lack of a consistent pathogenic process. Thus, a novel targeted macrophage therapeutic paradigm, which interferes with the signaling of pro-inflammatory cytokines, is required.

Ferroptosis is a newly discovered form of programmed cell death associated with iron-mediated lipid free radical accumulation and dysregulation of antioxidant responses [11]. Ferroptosis is involved in the pathophysiological progression of cancer [12], cardiovascular diseases [13], and infections [14]. LPS and Poly I:C are sufficient to cause severe oxidative stress, with excessive generation of reactive oxygen species (ROS) [15] and an increase in ferrous iron (Fe<sup>2+</sup>) in the labile iron pool [16], which can catalyze the production of ROS via Fenton chemistry, leading to oxidative stress. Corroborating these experimental findings, patients with CS present with elevated serum ferritin, a heteropolymetric protein complex composed of 24 ferritin heavy/ferritin light (FTH/FTL) subunits that can store and convert Fe<sup>2+</sup> into inert Fe<sup>3+</sup> through the ferroxidase activity of FTH to counteract the disrupted cellular iron homeostasis [17]. The role of ferroptosis in CS is attracting increasing attention.

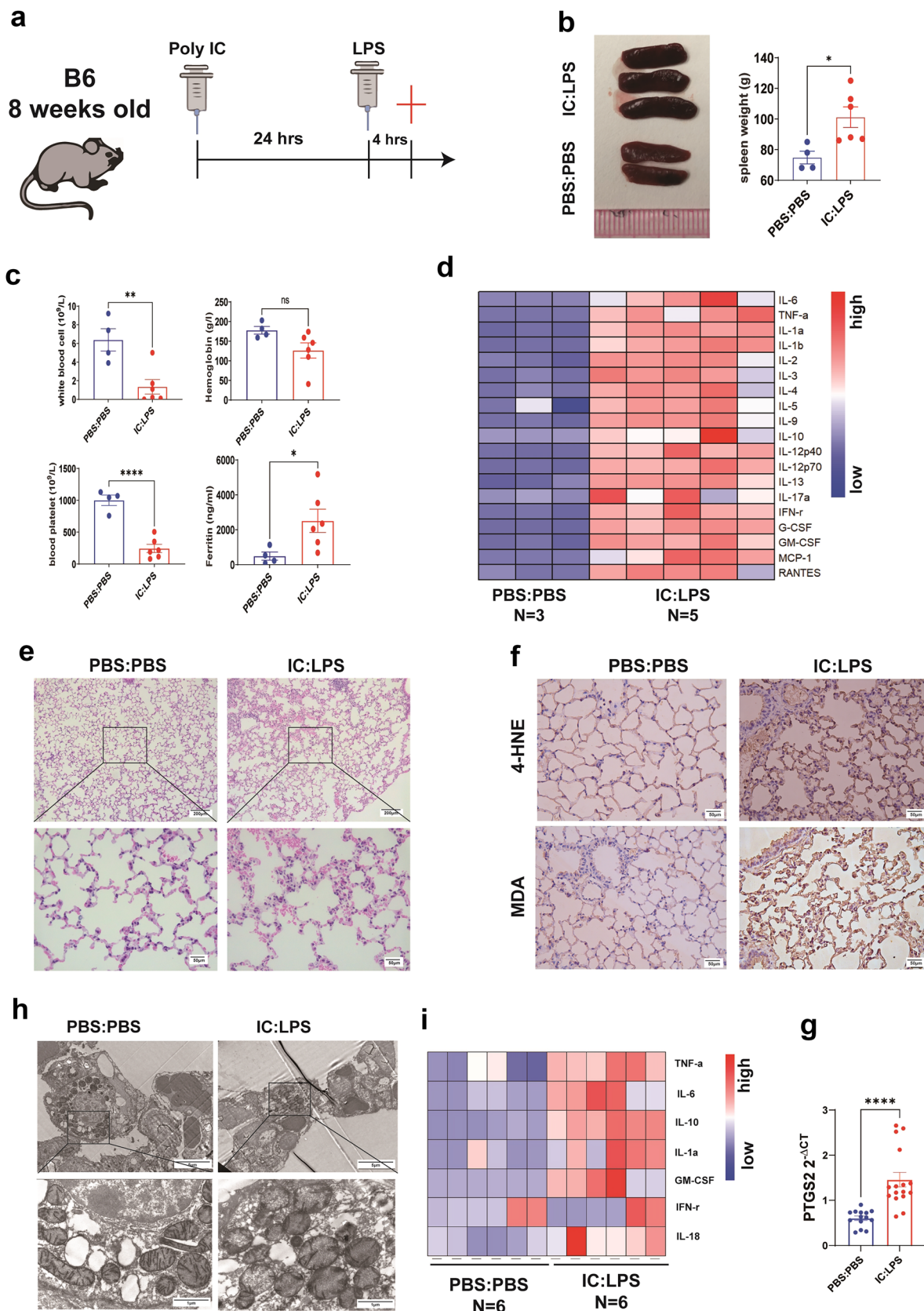
**Fig. 1** Cytokine storm associated with acute lung injury induced by Poly I:C and LPS exhibits significant ferroptosis (a) Experimental protocol. LPS(5 mg/kg) was injected intraperitoneally at 24 h after poly I:C (10 mg/kg) injection. Mice were scarified 4 h after the second challenge. Splenomegaly (b), blood routine test (c), plasma ferritin (e) and plasma cytokines (d) were measured. H&E staining (e), immunohistochemical staining of 4-HNE and MDA (f) in lung sections were measured. G. qRT-PCR analysis of PTGS2 in lung cells. Gene expression was normalized to Gapdh. H. Mitochondrial morphology was measured in lung sections using transmission electron microscopy. I. Heatmap of qRT-PCR analysis of cytokine gene expression in lung cells. Gene expression was normalized to Gapdh. Data are represented as mean  $\pm$  SD.  $P < 0.05$  was considered significant. \* $P < 0.05$ , \*\* $P < 0.01$ , \*\*\* $P < 0.0001$ .

However, previous studies have mostly focused on the key pathways of ferroptosis, including mitochondrial ROS, GPX4, and GSH/GSSH. Concurrently, the sensitivity of ferroptosis seems to be highly dependent on the state of cellular lipid [18] and amino acids [19] metabolism. Some studies have suggested that the inhibition of hexokinase (HK; an enzyme in anaerobic glycolytic metabolism) by 2-deoxy-d-glucose (2-DG)[20] or glucose starvation could substantially inhibit lipid peroxidation and ferroptosis [21]. However, the exact mechanism of glucose metabolism involved in ferroptosis during CS remains elusive.

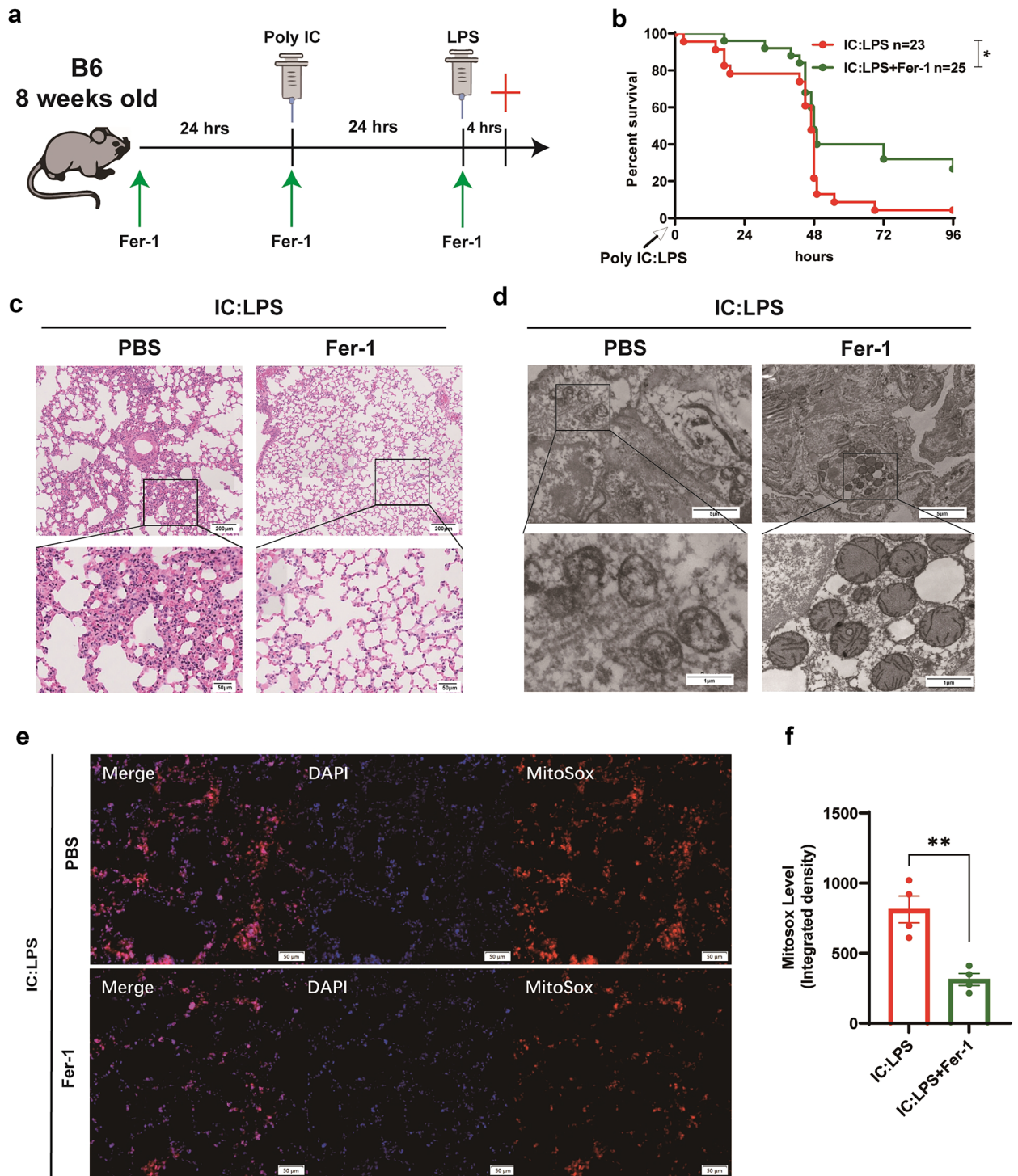
Conventionally, glycolysis is preferentially exploited by pro-inflammatory macrophages, in which pyruvate kinase M2 (PKM2) is a critical enzyme. Previously, Wang *et al.* showed that tumor cells undergoing ferroptosis have substantially lower PKM2 enzyme activity [22]. PKM2 is known to exist in two conformations: a tetramer, which is cytosol-localized and functions as enzymatically active as a pyruvate kinase, and a dimer form, which is enzymatically less active than the tetrameric isoform [23] and can translocate into the nucleus, wherein it can interact with HIF1 $\alpha$  to regulate glycolytic gene expression [24]. These conformations may be interconverted in response to specific stimuli or injuries. Furthermore, PKM2 tetramerization may reduce ROS levels [25] and correct the pro-inflammatory phenotype of macrophages in coronary artery disease [26]. However, whether conformational changes in PKM2 can regulate ferroptosis-associated ALI remains unknown.

Herein, we aimed to demonstrate the underlying mechanism by which ML-265, a small-molecule activator, affects CS-related ALI by inhibiting ferroptosis through the induction of tetrameric PKM2. Our results demonstrate the remarkable plasticity of glucose metabolism in macrophages, suggesting new ways of facilitating the resolution of ferroptosis in CS-related ALI.

PKM2 Nuclear Translocation Regulate Ferroptosis-Associated ALI









◀**Fig. 2** Fer-1 treatment attenuated IC:LPS-induced lung injury in mice (a) Experimental protocol. LPS(5 mg/kg) was injected intraperitoneally at 24 h after poly I:C (10 mg/kg) injection. Where indicated, the mice were administered a daily intraperitoneally of Fer-1(2.5 mg/kg) for three consecutive days, starting one day before poly I:C treatment. Mice were scarified 4 h after the second challenge. (b) Survival of animals challenged with IC:LPS between two groups. H&E staining (c) and mitochondrial morphology (d) in lung sections were measured. Confocal imaging (e) and quantification (f) of mitoxox (red) labeling in the lung. Data are represented as mean  $\pm$  SD.  $P < 0.05$  was considered significant. \* $P < 0.05$ , \*\* $P < 0.01$ .

## RESULTS

### Cytokines Storm Associated Acute Lung Injury Induced By Poly I:C and LPS Exhibit Significant Ferroptosis

Compared with the most common LPS-induced lung injury model, there has been no research on lung injury and ferroptosis involvement in a mouse model sequentially challenged with poly I:C and LPS (Fig. 1a). Consistent with a previous report [6], the IC:LPS model showed splenomegaly (Fig. 1b), leukopenia (Fig. 1c), thrombocytopenia (Fig. 1c), and dramatically elevated levels of ferritin (Fig. 1c) and serum pro-inflammatory cytokines (Fig. 1d). This model exhibited features of ALI, including widened alveolar septa, fluid accumulation within the alveolar space, and inflammatory cell infiltration (Fig. 1e). Moreover, the IC:LPS model displayed notably higher levels of 4-hydroxynonenal (4-HNE) and malondialdehyde (MDA) compared to that displayed by the control mice (Fig. 1f). In addition, the mRNA expression of prostaglandin-endoperoxide synthase-2 (Ptgs2), another typical feature of ferroptosis [27], was elevated in the IC:LPS model (Fig. 1g). Concurrently, we examined changes in mitochondrial morphology, a crucial event in ferroptosis execution [28]. Electron microscopy of lung cells revealed shrunken mitochondria, disruption of the inner cristae, and rupture of the outer membrane (Fig. 1h). Heightened ferroptosis rate was accompanied by an increased level of *in situ* expression of inflammatory cytokines in the lungs (Fig. 1i).

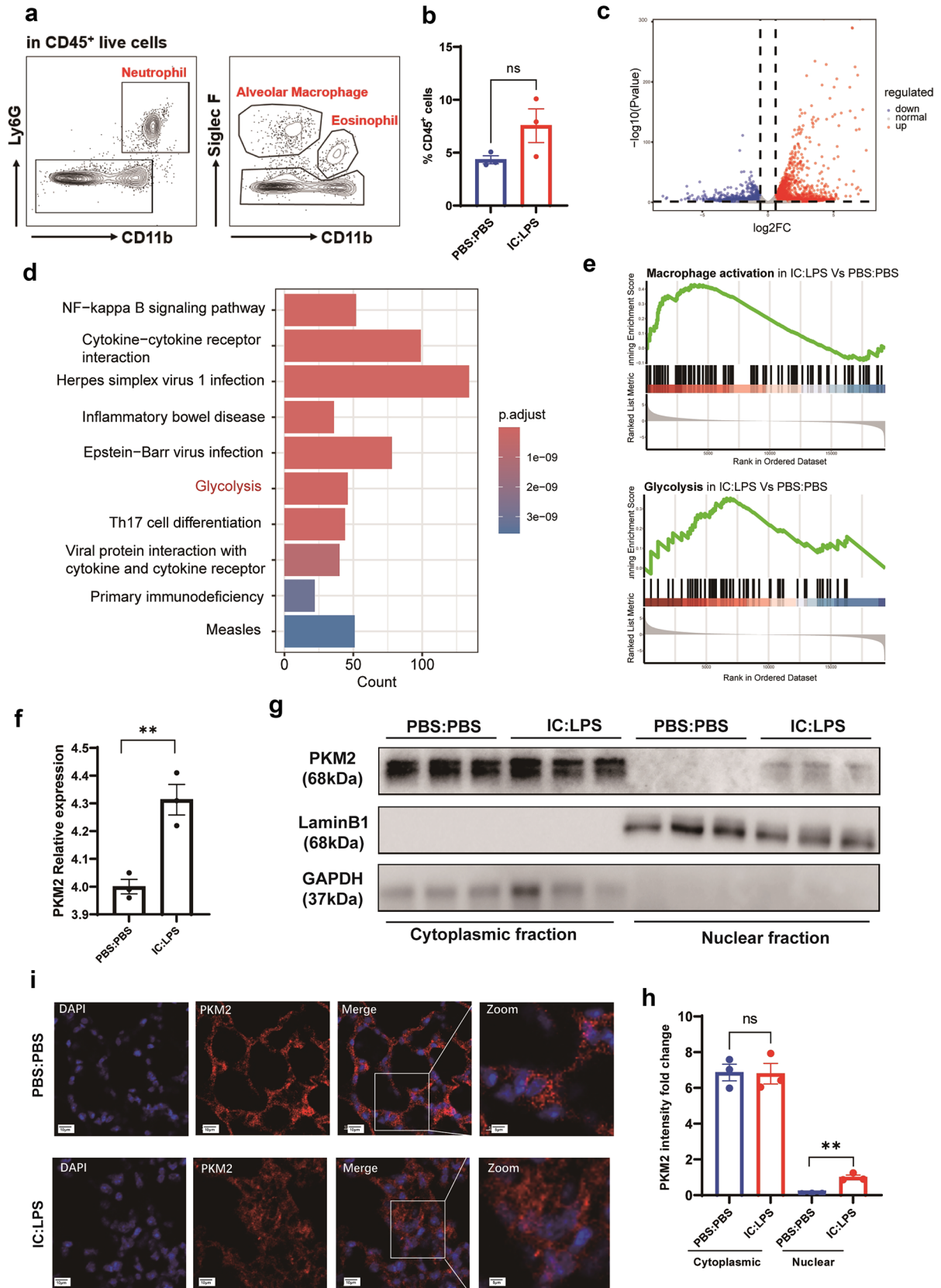
### Fer-1 Treatment Attenuated IC:LPS-Induced Lung Injury in Mice

To investigate the relative contribution of ferroptosis in IC:LPS-induced CS model related-ALI, we measured systemic inflammatory responses and survival in mice in the absence or presence of ferroptosis

inhibitor (ferrostatin-1, a synthetic antioxidant; Fer-1 [29]). Mice underwent a 3-day Fer-1 treatment starting a day before poly: IC administration (Fig. 2a). In comparison to the high mortality rate observed within 96 h after IC:LPS challenge, the survival rate increased to 30% in Fer-1 treated mice ( $p = 0.021$ ) (Fig. 2b). Concurrently, Fer-1 mitigated the histopathological lesions, which manifested as reduced inflammatory cell infiltration and diminished alveolar collapse (Fig. 2c). The Fer-1 treatment group exhibited enhanced mitochondrial morphology (Fig. 2d), along with a notable reduction in mitochondrial ROS levels, as measured using MitoSox Red (Fig. 2e, f). To further verify the role of ferroptosis in IC:LPS-induced lung injury, we used another specific and mechanistically distinct ferroptosis inhibitor (deferasirox; an oral iron chelator) in our mouse model (Supplemental Fig. 1a) and similarly found that deferasirox treatment could reduce mortality by 20% (Supplemental Fig. 1b) while alleviating histopathological lung injury and mitochondrial damage (Supplemental Fig. 1c, d). Our results revealed that the IC:LPS-induced CS resulted in significant lung injury and increased ferroptosis. However, this change was reversed by the ferroptosis inhibitor treatment.

### Alveolar Macrophage (AM) Exhibit Enhanced Glycolysis and PKM2 Translocation in IC:LPS-Induced ALI

Activated immune cells, such as macrophages, possess the ability to shift their energy metabolism from oxidative phosphorylation to glycolysis [6]. This metabolic switch directly influences the regulation of the inflammatory response. However, the relationship between inflammatory response, glycolysis, and ferroptosis remains unclear. To discern transcriptional variations, we conducted bulk RNA-seq on AM obtained from IC:LPS-induced model and control group (Fig. 3a). While the percentage of AM in the IC:LPS group exhibited an increasing trend in lung infiltration compared to that in the PBS group, the difference was not statistically significant (Fig. 3b). We identified differentially expressed AM genes between the two groups and focused our analyses on differentially activated pathways (Fig. 3c, d). AM in the IC:LPS group exhibited upregulation of inflammatory pathways accompanied by an elevation in glycolysis (Fig. 3d, e). In contrast, AM downregulated the inflammatory pathways in mice treated with IC: LPS plus Fer-1 (data not shown).



◀**Fig. 3** Alveolar macrophages exhibit enhanced glycolysis and PKM2 translocation in IC:LPS-induced ALI (a) Gating strategy for the sorting of AM (CD45<sup>+</sup> Ly6G<sup>-</sup> Siglec F<sup>+</sup> CD11b<sup>int/lo</sup>) for RNA-seq. (b) Percentage of AM in CD45<sup>+</sup> cells in lung. (c) Volcano plot showing DEGs of AM between IC:LPS treated and PBS:PBS treated groups. (d) Pathway analysis between IC:LPS treated and PBS:PBS treated groups. (e) Upregulation of inflammatory and glycolysis pathways of AM in the IC:LPS group compared with PBS:PBS treated group. (f) Expression of PKM2 in AM. (G-H) Western blot analysis of PKM2 expression in cytoplasmic and nuclear fraction of AM. (I) Confocal imaging of PKM2 (red) and DAPI (blue) labeling in the lung. Data are represented as mean ± SD. P < 0.05 was considered significant. \*\*P < 0.01.

Since the metabolic analyses of AM revealed a preference for glycolysis, we further examined the metabolic enzymes involved in this pathway. PKM2, which governs the last step of glycolysis, is a rate-limiting enzyme. There are two isoforms of pyruvate kinase M (PKM1 and PKM2) [30]. Recent studies have revealed that PKM2 contributes to the activation of macrophages and release of inflammatory factors [31]. Growing evidence suggests that the transition from PKM2 tetramer to PKM2 monomer/dimer (nuclear translocation) plays a crucial role in promoting inflammatory responses [32]. In our comparison of the two isoforms, we observed a significantly higher expression level of PKM2 in the IC:LPS group compared with that in the control group (Fig. 3f). To validate the RNA-seq results of RNA sequencing, western blotting and immunofluorescence staining were performed to measure the expression pattern of PKM2 in AM. Subcellular fractionation showed that nuclear PKM2 expression increased in the IC:LPS group, whereas the cytoplasmic fraction remained unchanged (Fig. 3g, h). Immunofluorescence confirmed the nuclear localization of PKM2 (Fig. 3i). These findings imply that the pathological progression of IC:LPS-induced ALI may be linked to increased translocation of PKM2, triggering an inflammatory response.

### Inhibition of PKM2 Nuclear Translocation Alleviates Lung Injury and Ferroptosis in IC:LPS Model

To further determine the effect of PKM2 nuclear translocation on lung injury in the IC:LPS model, mice were treated with IC:LPS with or without ML-265 (a PKM2 monomer/dimer inhibitor) [23] (Fig. 4a). The treatment of ML-265 abolished the nuclear localization of PKM2 in AM, as confirmed by immunoblotting (Fig. 4b) and confocal microscopy (Fig. 4c). Mice treated with

ML-265 were resistant to mortality induced by IC:LPS, similar to the previously observed dramatic improvement in survival with 2-DG [6], indicating that PKM2-mediated glycolysis contributes to the fatal outcome associated with the CS (Fig. 4d). The survival change in the ML-265 group was accompanied by improved pathological changes (Fig. 4e) and decreased levels of inflammatory cytokines in the lungs (Fig. 4f).

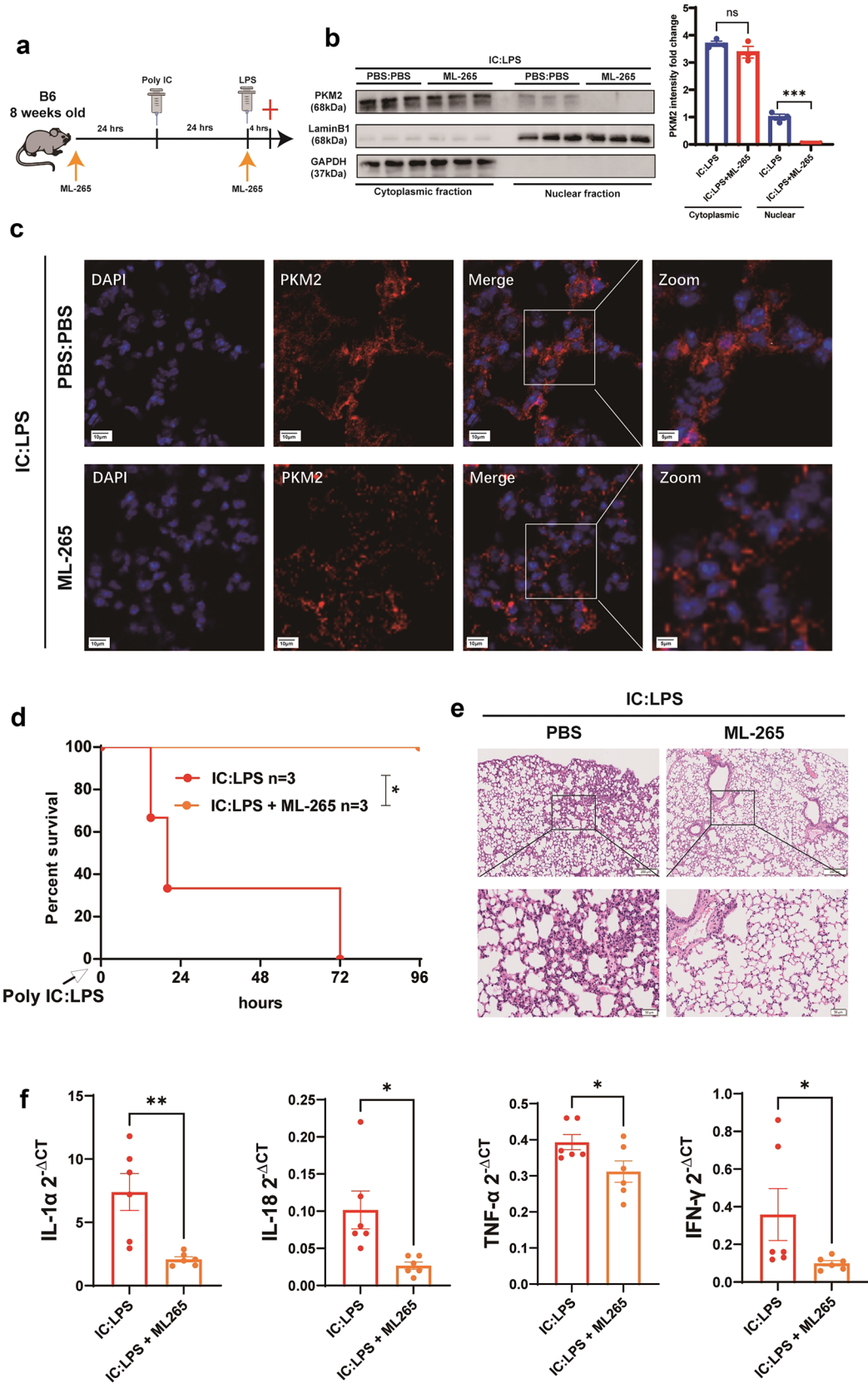
Next, we investigated whether the inhibition of PKM2 nuclear translocation could rescue ferroptosis. Mice pretreated with ML-265 exhibited a noteworthy decrease in the expression of 4-HNE compared to those treated with PBS (Fig. 5a, b). In addition, the ML-265 group exhibited a downregulation in the mRNA level of Ptg2 (Fig. 5c) and an improvement in mitochondrial morphology in the lungs (Fig. 5c, d). The effect of ML-265 on the metabolic flux in lung cells was further assessed using seahorse assays. The evaluation of glycolysis through the ECAR revealed that both Fer-1 and ML-265 significantly reduced the glycolytic capacity (Fig. 5e). In contrast, the OCR, as measured by the maximal respiration capacity (MRC), was not significantly different between the IC: LPS and IC: LPS + Fer-1 control groups. However, ML-265 treatment resulted in a significant increase of MRC compared to IC: LPS group (Fig. 5e).

These data suggest that, in the IC:LPS-induced CS model, the administration of ML-265 resulted in the formation of a highly active tetrameric PKM2, leading to improved survival and attenuation of ALI. Furthermore, ML-265 treatment decreased ferroptosis and restored the balance between anaerobic glycolysis and oxidative phosphorylation.

### PKM2 Nuclear Translocation Associated with Circulating Inflammation in Patients with Lung Infection

Classical CD14<sup>+</sup> blood monocytes migrate into the lung tissue and give rise to human AM during inflammation [33]. Therefore, to further evaluate PKM2 nuclear translocation in CS-related ALI in humans, we performed a detailed multiparametric study combining transcriptomic analyses, flow cytometry, and immunofluorescence in CD14<sup>+</sup> cells from PBMCs (Fig. 6a). Our study consisted of a cohort of 14 patients diagnosed with lung infection based on HRCT scans, with 9 of these patients exhibiting distinct characteristics suggestive of CS [34] (Table 1). Among the 9 patients, seven were





## PKM2 Nuclear Translocation Regulate Ferroptosis-Associated ALI

**Fig. 4** Inhibition of PKM2 nuclear translocation alleviates lung injury in IC:LPS model (a) Experimental protocol. LPS(5 mg/kg) was injected intraperitoneally at 24 h after poly I:C (10 mg/kg) injection. Where indicated, the mice were administered every other day intraperitoneally of ML-265 (50 mg/kg), starting one day before poly I:C treatment. Mice were scarified 4 h after the second challenge. (b-c) Western blot analysis of PKM2 expression in cytoplasmic and nuclear fraction of AM. (c) Confocal imaging of PKM2 (red) and DAPI (blue) labeling in the lung. (d) Survival of animals challenged with IC:LPS between two groups. (e) H&E staining in lung sections were measured. (f) qRT-PCR analysis of cytokine gene expression in lung cells. Gene expression was normalized to Gapdh. Data are represented as mean  $\pm$  SD.  $P < 0.05$  was considered significant. \* $P < 0.05$ , \*\* $P < 0.01$ , \*\*\* $P < 0.001$ .

confirmed to have SARS-CoV-2 infection, while two were confirmed to have cytomegalovirus infection. Additionally, we included a control group consisting of three healthy controls.

We isolated CD14<sup>+</sup> cells from PBMCs (n = 3 in the healthy controls and n = 3 in CS infection groups) and generated RNA-seq data. We identified differentially expressed genes between the two groups (Fig. 6b). CD14<sup>+</sup> blood monocytes in patients with CS exhibited an upregulation of ferroptosis accompanied by an increase in glycolysis (Fig. 6c), which is consistent with the results of our *in vivo* models. Intracellular expression of PKM2

in peripheral blood CD14<sup>+</sup> monocytes was significantly higher in patients presenting with CS than in healthy controls (Fig. 6d). Immunofluorescence further confirmed that elevated intracellular PKM2 levels in these patients were accompanied by an increase in nuclear translocation (Fig. 6e). To determine whether PKM2 nuclear translocation can also occur in other white blood cells—T cells, B cells, and neutrophils, we performed immunofluorescence analysis of peripheral blood samples and did not find significant PKM2 nuclear translocation regardless of the patients of lung infection with or without CS (Supplemental Fig. 2). Furthermore, Correlation analysis also suggested a positive association between PKM2 expression in peripheral blood CD14<sup>+</sup> monocytes and inflammatory markers, including serum IL-6, ferritin, and PCT (Fig. 6f), in patients with acute respiratory infection.

## DISCUSSION

The COVID-19 pandemic revived research into CS. Ferroptosis may exacerbate the progression of the inflammatory response in macrophages [35–37]. Recently, macrophage metabolic reprogramming, particularly glycolysis, has emerged as a promising

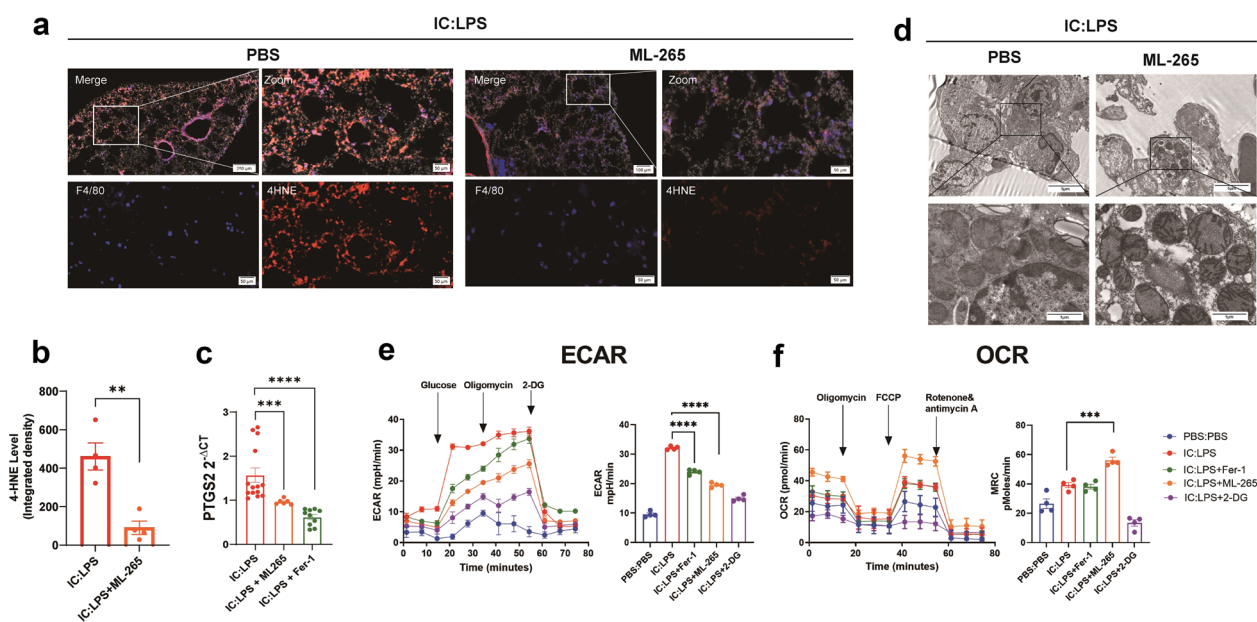


**Fig. 5** Inhibition of PKM2 nuclear translocation alleviates ferroptosis in IC:LPS model (a-b) Confocal imaging of 4-HNE (red) and F4/80 (blue) labeling in the lung. (c) qRT-PCR analysis of PTGS2 in lung cells. Gene expression was normalized to Gapdh. (d) Mitochondrial morphology in lung sections were measured. (e-f) The ECAR and OCR were measured in lung cells of mice in different groups by using a Seahorse XF96e Extracellular Flux analyzer. Data are represented as mean  $\pm$  SD.  $P < 0.05$  was considered significant. \*\* $P < 0.01$ , \*\*\* $P < 0.001$ , \*\*\*\* $P < 0.0001$ .

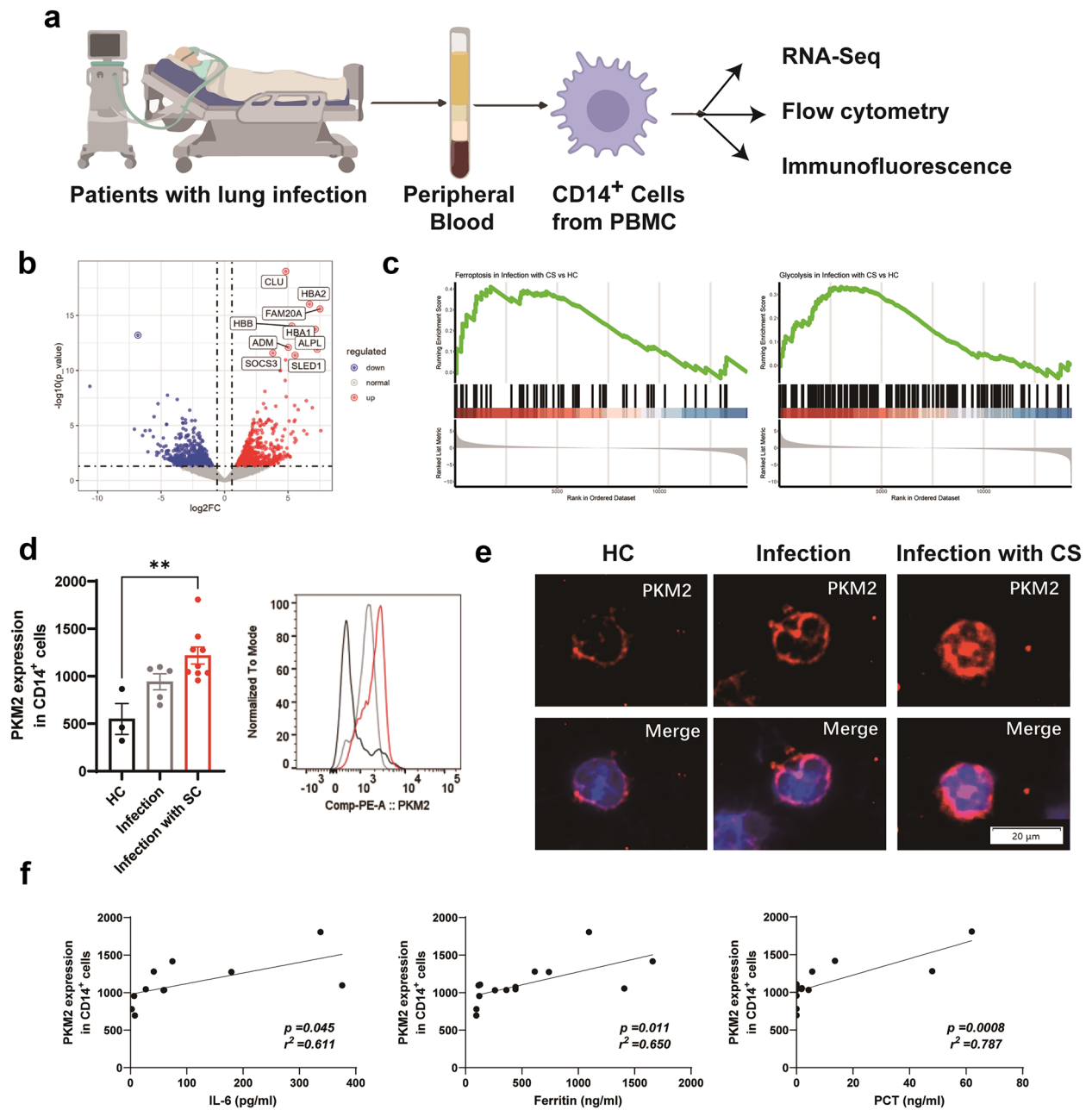


**Fig. 6** PKM2 nuclear translocation associated with circulating inflammation in patients with lung infection (a) Experimental protocol. Peripheral blood of 14 patients diagnosed with lung infection and 3 healthy controls (HC) were collected. CD14<sup>+</sup> cells were isolated from PBMCs and further analyzed using RNA-Seq, flow cytometry, and immunofluorescence. (b) Volcano plot showing DEGs of CD14<sup>+</sup> cells between lung infection patients with CS and healthy controls. (c) Upregulation of ferroptosis and glycolysis pathways of CD14<sup>+</sup> cells in lung infection patients with CS compared with healthy controls. (d) Flow analysis (MFI value) of PKM2 expression in CD14<sup>+</sup> cells. (e) Confocal imaging of PKM2 (red) and DAPI (blue) labeling in CD14<sup>+</sup> cells. (f) Correlation of PKM2 expression in CD14<sup>+</sup> cells with inflammatory parameters (IL-6, ferritin and PCT). Data are represented as mean  $\pm$  SD.  $P < 0.05$  was considered significant. \*\* $P < 0.01$ .



## PKM2 Nuclear Translocation Regulate Ferroptosis-Associated ALI

**Table 1** Baseline characteristics of healthy controls, lung infection patients and lung infection with cytokine storm

Variable <sup>b</sup>	Healthy controls (n = 3)	Lung infection (n = 5)	Lung infection with cytokine storm (n = 9)	P value*
Male, n (%)	3 (100.0)	3 (60.0)	9 (100.0)	0.999
Age (year), mean (SD)	38.0 (10.8)	70.8 (7.8)	72.7 (12.3)	<0.001
Evidence of pathogens, n (%) <sup>a</sup>				
Bacterial	0 (0.0)	4 (80.0)	8 (88.9)	
Viral	0 (0.0)	1 (20.0)	9 (100)	
Fungal	0 (0.0)	0 (0.0)	1 (11.1)	
<b>Entry Criteria</b>				
Positive for COVID-19, n (%)	0 (0.0)	1 (20.0)	7 (77.8)	<0.001
Ferritin (ug/L), median (IQR)	20 (2, 45)	115 (95, 1408)	443 (121, 1660)	<0.001
C-reactive protein (mg/L), median (IQR)	5 (1, 8)	85 (9, 135)	120 (59, 205)	<0.001
<b>Optional Criteria</b>				
Albumin (g/L), median (IQR)	45.0 (42.5–48.5)	28.6 (27.4–31.5)	22.7 (18.6–29.6)	<0.001
Lymphocytes (10 <sup>9</sup> /L), median (IQR)	2.44 (2.44–4.33)	1.5 (1.5–2.1)	0.8 (0.6–0.9)	<0.001
Neutrophil (10 <sup>9</sup> /L), median (IQR)	1.3 (1.3–1.7)	5.4 (4.3–12.2)	12.4 (9.7–18.7)	<0.001
AST (mg/L), median (IQR)	13.00 (12.00–16.00)	28.0 (21.0–29.0)	62.0 (39.0–72.0)	0.024
D-dimers > 600 (mg/L), n (%)	0 (0.0)	1 (20.0)	5 (55.5)	0.414
LDH (mg/L), median (IQR)	85.0 (77.5–87.5)	217.0 (160.0–298.0)	348.0 (278.0–374.0)	0.017
Troponin I (ng/L), median (IQR)	0.01 (0.01–0.01)	0.01 (0.01–0.2)	1.0 (0.3–1.5)	0.007
BUN: creatinine ratio, median (IQR)	14 (13–15)	19 (17–23)	25 (21, 28)	0.024
Procalcitonin (ng/L), median (IQR)	0.03 (0.03–0.05)	4.27 (0.02–13.60)	4.27 (0.02–13.60)	0.012
ESR (mm/h), median (IQR)	8.0 (8.0–9.0)	27.0 (23.0–60.0)	35.0 (32.0–45.0)	<0.001
IL-6 (pg/L), median (IQR)	2.3 (2.0–2.9)	13.6 (7.8–22.3)	60.0 (41.4–74.5)	<0.001

HRCT, high-resolution computed tomography; AST, Glutamic oxalic aminotransferase; ESR, erythrocyte sedimentation rate; LDH, lactate dehydrogenase; BUN, Blood Urea Nitrogen

\*P-values were calculated to compare the differences between the Healthy and Infection with cytokine storm groups. Comparison of continuous variables using student-t test and Mann–Whitney nonparametric test. Categorical variables were compared using chi-squared test or Fisher exact test

<sup>a</sup>Twelve cases were identified as bacterial infections, including 4 with *Streptococcus pneumoniae*, 3 with *Enterococcus faecium*, and 5 with *Klebsiella pneumoniae*. Viral infections totaled 10 cases, with 8 attributed to the COVID-19 and 2 to cytomegalovirus. One case was a fungal infection, caused by *Cryptococcus neoformans*

<sup>b</sup>Data are presented as median (interquartile range) or mean (standard deviation)

therapeutic strategy for combating ferroptosis during the CS [38, 39]. However, the correlation between CS associated with an ALI and ferroptosis remains unclear. In the current study, we demonstrated that ferroptosis inhibitors are particularly efficient at mitigating CS-associated ALI and improving survival. Importantly, we found that PKM2 translocates to the nucleus, enhancing the glycolytic metabolism of macrophages under different TLR stimulation conditions. Our study also demonstrated that treatment with ML-265 (an inhibitor of the tetrameric conformation of PKM2) markedly inhibited PKM2 nuclear entry and consequently suppressed ferroptosis (Fig. 7). In summary, this study

provides novel insights into the non-canonical metabolic function of PKM2 in the modulation of ferroptosis and may aid in the development of drugs for the treatment of CS-associated lung injury.

Ferroptosis is a form of immunogenic cell death that can trigger inflammatory responses by releasing DAMPs [40], which may play an important role in hyperinflammation such as the CS. Accordingly, ferroptosis may be involved in multiple system diseases, e.g., acute kidney injury [41], ALI [42] and ischaemia–reperfusion injury (IRI) [11]. Consistent with previous studies, our findings confirmed ferroptosis activation in the mouse model by poly (I:C) and LPS challenge, mimicking severe

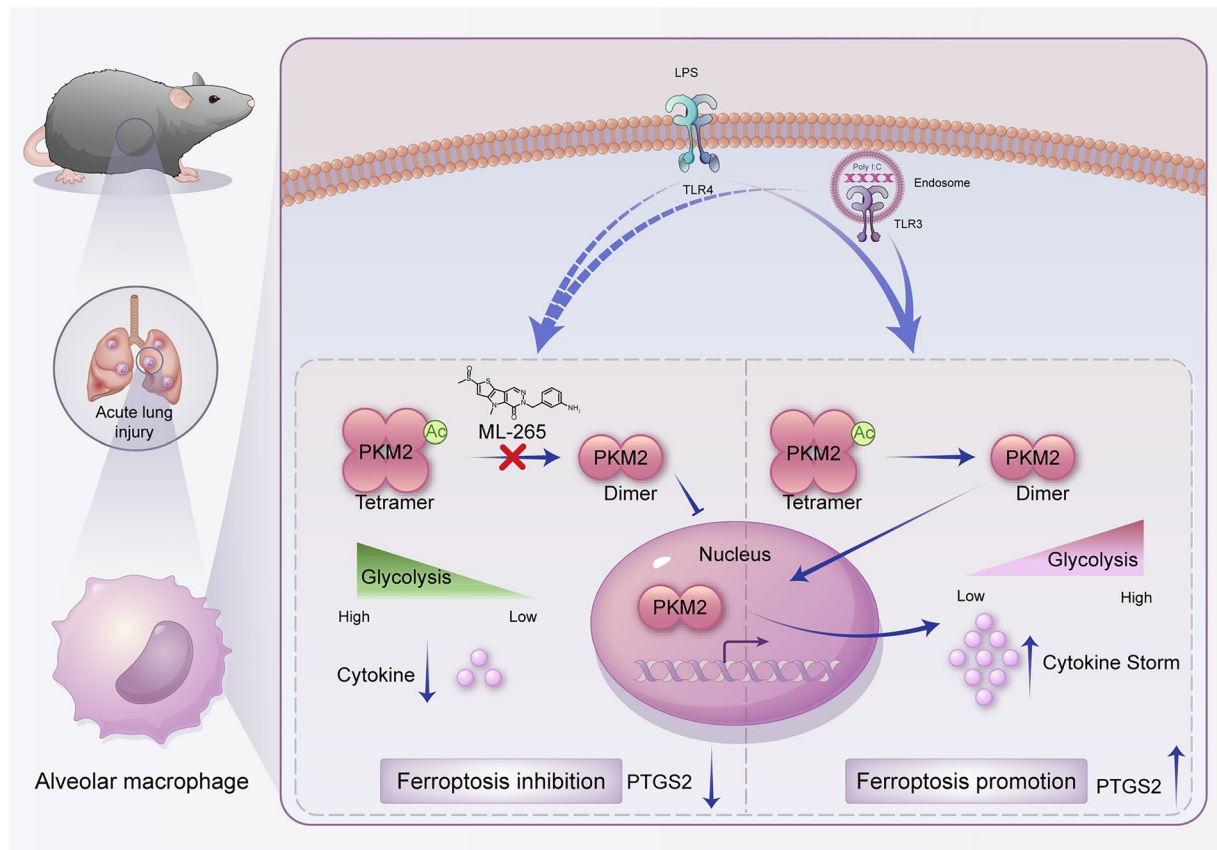


**Fig. 7** Schematic diagram of the study. Poly I:C (TLR3) and LPS (TLR4) stimulation increases glycolysis and leads to translocation of glycolytic enzyme PKM2 dimer into the nucleus of alveolar macrophage, which induces pro-inflammatory cytokine genes and ferroptosis genes expression. Induction of tetrameric PKM2 by ML-265 blocks its nuclear translocation and engagement of glycolysis, inhibiting ferroptosis and cytokine storm, and development of lung injury *in vivo*.

infections in patients, via MDA and 4-NHE staining, and an immunofluorescence assay. Thus, agents that inhibit ferroptosis are promising new options for the treatment of the CS. Indeed, some strategies for inhibiting ferroptosis have shown potential as COVID-19 treatments. Two ferroptosis inhibitors, rosiglitazone (an ACSL4 inhibitor) and rosiglitazone, can reduce the viral yield of coronaviruses, including SARS-CoV-2 [43]. However, their use has raised major safety concerns, including increased risk of myocardial infarction, stroke, edema, congestive heart failure, reduced bone mineral density, increased fracture rate, and death [44], limiting their clinical application. Meanwhile, deferoxamine and deferiprone may alleviate hyper-ferritinemia by scavenging excess iron from the body in SARS-CoV-2 infection resulting in cytokine release syndrome [45, 46]. However, the clinical utility of iron chelation in ameliorating the CS has only been

shown in small pilot studies, and evidence from large clinical trials remains lacking [47].

Elevated PTGS2 transcription is a hallmark of ferroptosis in malignant neoplasms [48], inflammatory [49], neurological diseases [50]. In addition, PTGS2 may mediate ferroptosis in neural cells after traumatic injury [51]. The chemical inhibition of system Xc<sup>-</sup> by erastin (a prototype trigger of ferroptosis) also results in PTGS2 upregulation in cancer cells [52]. Herein, we found that poly I:C and LPS insults resulted in leukopenia and thrombocytopenia; an upregulation of 4HNE, MDA, and PTGS2 mRNA levels; lung tissue injury; and pro-inflammatory factor abnormalities. Dang *et al.* recently reported that PKM2-activated macrophages drive abdominal aortic aneurysm progression by promoting vascular lipid peroxidation and ameliorating macrophage antioxidant capacity in vascular adventitia, as evidenced by increased gene

expression of *Ptgs2* and decreased gene expression of *Gpx4* and *Slc7a11* [53]. The mechanism may be related to PKM2, which facilitates the accumulation of iron and consequent ferroptosis. In contrast, Wang *et al.* found that tumor cells with downregulated PKM2 showed significant ferroptosis, which may account for the cellular metabolic pathway from glycolysis to OXPHOS, which has a profound impact on cellular ROS stress [22]. Overall, given the complexity of the mechanisms of ferroptosis and the specificity of PKM2 regulation in different cell types, whether other mechanisms exist through which PKM2 may induce ferroptosis-related genes expression requires further research.

A tightly controlled PKM2 conformation balance among PKM2 tetramers, dimers, and monomers is critical for PKM2 functions [54]. In an inflammatory context, mitochondrial ROS promote destabilization of the PKM2 tetramer, favoring its dimerization and subsequent nuclear translocation in macrophages [55]. PKM2 nuclear entry exerts different functions, such as histone phosphorylation [56] and regulation of gene transcription, in addition to encoding enzymes involved in glycolysis, including *Glut1* and *Ldha* [57], also *Il1b* and *Il12* [26, 58]. Moreover, previous studies in tumor cells have demonstrated that dimeric PKM2 complexed with  $\beta$ -catenin, STAT3, Oct4, NF- $\kappa$ B/p65, and HIF-1 $\alpha$  to regulate the expression of target genes. However, other phenotypic mechanisms controlled by the nuclear function of PKM2 remain unexplored. In this study, we established a positive correlation between PKM2 nuclear entry and ferroptosis, which was reversed by treatment with a pharmacological dimeric PKM2 inhibitor. Notably, Leu and colleagues found that the treatment of cells with TEPP46, another pharmacological dimeric PKM2 inhibitor (akin to ML-265), reversed the increased ferroptotic cell death rate caused by glutamate [59]. Additionally, our RT-PCR assay demonstrated that the inhibition of dimeric PKM2 was significantly associated with decreased transcript expression of *PTGS2*. Whether the presence of dimeric PKM2 in the nucleus of macrophages facilitates transcription of ferroptosis sensitivity genes remains to be addressed.

## CONCLUSION

In conclusion, as a critical enzyme in glycolysis, dimeric PKM2 nuclear entry contributes to the expression of pro-inflammatory cytokines and ferroptosis activation. We established that the treatment of mice with ML-265

induced PKM2 to form a highly active tetrameric form, rebalancing anaerobic glycolysis and oxidative phosphorylation. PKM2 assists ferroptosis-related gene expression and may participate in ferroptosis activation during the CS. Notably, in PBMC from patients with a lung infection, PKM2 fluorescence in the nucleus was correlated with increased pro-inflammatory cytokine expression level. We propose that PKM2 is a key regulatory node that integrates metabolic reprogramming with intranuclear functions to regulate ferroptosis. Targeting PKM2 could be explored as a potential means of preventing or alleviating the hyper-inflammatory state or CS syndrome with aberrant ferroptotic cell death.

## MATERIAL AND METHODS

### Animals

Eight-week-old male C57Bl/6 (WT) mice were purchased from Shanghai SLAC Laboratory Animal Co. Ltd. Isoflurane was used to anesthetize the animals to minimize their suffering. Animal experiments were performed in accordance with the Guide for the Care and Use of Laboratory Animals issued by the Ministry of Science and Technology of China. The study protocol was approved by the Institutional Animal Care and Use Committee of Shanghai Jiao Tong University School of Medicine (Permit Number: A-2019-041).

### Cytokine Storm Model

The CS model was induced by sequential challenge with poly I:C and LPS, as previously described [6]. Briefly, mice were intravenously injected with 10 mg/kg of high-molecular-weight poly I:C (InvivoGen). LPS derived from *Escherichia coli* 055:B5 (Sigma-Aldrich) diluted in phosphate-buffered saline (PBS) was injected intraperitoneally at 5 mg/kg 24 h after poly I:C injection. Mice were administered ferrostatin-1 (Fer-1, Selleck Chemicals) at 2.5 mg/kg by intraperitoneal injection [13], ML-265 (PKM2 monomer/dimer inhibitor, absin) at 50 mg/kg by intraperitoneal injection [60] or deferasirox (iron chelator, Deferasirox Dispersible Tablets, Novartis Pharma Schweiz) at 10 mg/kg by gavage [61]. The control group was treated with PBS. The plasma cytokines levels were measured using the Bio-Plex Pro Mouse Chemokine Panel 23-plex kit according to the manufacturer's protocols (BIO-RAD).



## Cytokine and Metabolic Genes Expression

Single-cell suspensions were prepared from spleens and lungs using standard procedures [62]. After red blood cell lysis, cells were used for RNA extraction. Total RNA was isolated from the cells using TRIzol reagent (Invitrogen), and cDNA was synthesized using a high-capacity cDNA reverse transcription kit (Invitrogen). Quantitative real-time PCR was conducted using TB Green on the Roche LightCycler 480 system. The primers used for the indicated genes are listed in Supplemental Table 1.

## Histology, Immunohistochemistry, and Immunofluorescence

Fresh mouse lung tissue was fixed overnight in 2% paraformaldehyde. Tissue samples were embedded in paraffin and sectioned to slices 4- $\mu$ m-thick, followed by hematoxylin and eosin staining. For immunohistochemistry, the primary antibodies, 4-HNE (Abcam, 1:200) or MDA (Adipogen, 1:100), were incubated overnight at 4 °C. Staining was performed using the Vectastain Elite ABC kit and DAB peroxidase substrate kit (Vector Laboratories). The images were acquired using a Leica DM750 microscope (Leica ICC50 W) camera.

For immunofluorescence, lung slices were dewaxed with xylene, graded with ethanol to water, and antigens were repaired with a buffer (pH 6.0). After being rinsed three times for 5 min in TBS, the sections were sealed with a blocking buffer (0.3% Triton X-100, 1% BSA, 1% FBS, and 0.1 M Tris HCL) at room temperature, incubated with the aqueous solution, and then incubated overnight with rabbit anti-4-HNE antibodies (Alpha Diagnostic International, 1:200 dilution) or anti-PKM2 antibodies (CST, 1:200 dilution) at 4 °C. After three washes with PBS, the cells were incubated at room temperature with fluorescently labeled secondary antibodies for 1 h. Nuclei were subsequently stained with 6-diamino-2-phenylindole in the dark. For mitochondrial ROS detection, lung tissues were mixed with MitoSox at 100 nM (Invitrogen) for 15 min at 37 °C and then fixed in 2% paraformaldehyde for 15 min at 37 °C. The images were captured using a fluorescence microscope.

## Transmission Electron Microscopy

Fresh myocardium samples (1 mm  $\times$  1 mm  $\times$  1 mm) were quickly and carefully collected and placed in tubes containing a fixing solution for 4 h. Then, the lung tissue

samples were permeabilized, dehydrated, and embedded overnight. The samples were viewed using a Tecnai 10 Electron Microscope (FEI, Hillsboro, OR, USA) at the Electron Microscopy Core Facility, Shanghai Jiao Tong University School of Medicine.

## Flow Cytometry Sorting and Analysis

For AM sorting from the lung cells of the mouse model, the cells were first stained with an Fc blocker in MACS buffer (1  $\times$  PBS with 0.5% BSA, 2 mM EDTA). Then the cells were resuspended in 50  $\mu$ L MACS buffer with diluted indicated flow cytometry antibodies and incubated for 30 min at 4 °C. AM were gated as CD45<sup>+</sup> (APC Anti-Mouse CD45 antibody, clone 30-F11, Abcam) Ly6G<sup>-</sup> (PE-Cy7 Anti-Mouse Ly6G antibody, clone 1A8, Biolegend) CD11b<sup>lo-int</sup> (FITC Anti-Mouse/Human CD11b Antibody, clone M1/70, Biolegend) Siglec F<sup>+</sup> (PE Anti-Mouse Siglec-F, clone E50-2440, BD Pharmingen) live cells. Cells were washed twice with MACS buffer and sorted using a Beckman Coulter MoFlo Astrios EQ.

## Analysis of Extracellular Acidification rate (ECAR) and Oxygen Consumption rate (OCR) with the Seahorse XF Platform

Cellular and mitochondrial bioenergetics were measured using a Seahorse XF96 extracellular flux analyzer. Glycolysis and mitochondrial stress tests were performed according to manufacturer's instructions. For glycolysis stress test, cells were incubated in glucose-free Seahorse assay media supplemented with 1 mM pyruvate at 37 °C in an incubator without CO<sub>2</sub> for 1 h prior to the assay. Injectors were loaded to add 20 mM glucose, 1  $\mu$ M oligomycin and 100 mM 2 deoxy-glucose (2-DG). For the mitochondrial stress test, injectors were loaded with 20 mM glucose, 1  $\mu$ M oligomycin, 1  $\mu$ M FCCP, 1  $\mu$ M rotenone and 2  $\mu$ M antimycin A during mitochondrial stress test. The baseline ECAR and OCR values were averaged between technical replicates for the first three successive time intervals.

## Subcellular Fractionation

Subcellular fractionation was carried out to isolate nuclear-enriched lysates as previously described. First, a cell lysis buffer suspension was used to extract the

soluble cytoplasmic protein fraction. After incubation on ice for 10 min, samples were centrifuged. The supernatant containing the soluble cytoplasmic fraction was removed. The residual nuclei pellet was treated according to the manufacturer's instructions using Turbo DNase. Eventually, the complete solubilization of the nuclei was achieved by introducing nuclear lysis buffer, followed by its incubation at 4 °C for 10 min. The final step involved mechanical centrifugation of the samples and the subsequent collection of the supernatant comprising the nuclear lysate.

### Western Blot Analysis

Western blot analysis was performed on cells that were first lysed in RIPA buffer. The analysis was performed according to a previously described methodology. The samples were electrophoresed on either 7.5% or 10% gels and transferred onto PVDF membranes. The membranes were then blocked at room temperature with a 5% milk solution in TBS-Tween for a duration of 1 h prior to the commencement of primary antibody incubation, which was performed at 4 °C overnight. An HRP-conjugated secondary antibody was added and subsequently incubated at room temperature for 1 h. Final visualization of the western blots was achieved using chemiluminescence reagents.

### Clinical Cohort

We conducted a cohort study that included 14 patients diagnosed with a lung infection and three healthy controls at the Department of Emergency and Critical Care Medicine, Renji Hospital from April to September 2023. Nine patients presented distinct characteristics indicative of CS, as per the defined predictive criteria [34]. Lung infection patients enrolled in this study were all initial infections during hospitalization. Participants under the age of 18 years, pregnant women, with recurrent infections and those with a documented terminal illness, a history of malignant tumors, human immunodeficiency virus, autoimmune diseases, and diseases of the blood were excluded. During hospitalization, we recorded data on hospital admission, including demographic characteristics (sex and age), laboratory test results, pathogen details and treatment regimens. This study was approved by the Ethics Committee of Renji Hospital (KY2023-053-B).

### Human Peripheral Blood Cells Isolation and Analysis

Five-milliliter whole blood samples were obtained from patients on the day of admission and healthy volunteers using ACD tubes (BD Vacutainer) and fractionated over Ficoll gradients to obtain peripheral blood mononuclear cells (PBMCs).

CD14<sup>+</sup> cells were isolated from PBMCs using a positive selection kit (EasySep™ Human CD14 Positive Selection Kit II; STEMCELL). PBMCs or CD14<sup>+</sup> cells ( $1 \times 10^4$  cells- $5 \times 10^4$  cells) were centrifuged onto glass slides using a Cytospin 4 Cytocentrifuge (Thermo Scientific) and subsequently fixed for immunofluorescence staining targeting PKM2. Subsequently, cells were distinguished as neutrophils (Ly6G<sup>+</sup>), B cells (CD19<sup>+</sup>), or T cells (CD3<sup>+</sup>). The cell nuclei were stained with DAPI.

CD14<sup>+</sup> cells were also prepared for flowcytometry analysis. Briefly, the cells were permeabilized for 1 h using the FOXP3/transcription factor staining buffer set (Thermo Fisher Scientific) and then stained for 1 h with antibodies against PKM2 (CST, 1:200 dilution). The cells were washed twice with a MACS buffer and analyzed by flow cytometry. Data were acquired using a BD Fortessa X20 (BD Biosciences) and analyzed using the FlowJo software (Tree Star, Inc.).

### Library Preparation and RNA-Seq Analysis

In this study, three patients exhibiting CS and age-matched healthy controls were selected. CD14<sup>+</sup> cells were isolated from the individuals' peripheral blood samples. In addition, three mice each from the IC-LPS model group and the PBS control group were used in this study. Alveolar macrophages (AM) were extracted from these mice as previously outlined. RNA was then extracted from these samples, and 1 µg of total RNA was assessed for quality (RIN > 7) using an Agilent Bioanalyser 2100 system. This RNA sample was then used to build bar-coded sequencing libraries following the instructions of Illumina's TruSeq Stranded mRNA Library Prep Kit.

Raw RNA-seq data were analyzed using common RNA-seq analysis tools. The quality of the FastQ files was determined using FastQC version 0.11, which revealed Phred quality scores above 20 points, indicating a base call accuracy of 99%. Low-quality reads were trimmed using Trimmomatic, version 0.36. The RNA-seq

files were aligned to either the human or mouse reference genome (version hg38) using HISAT2 (version 2.2.1.0). Gene read counts were performed using HTSeq version 0.9.1. Differentially expressed genes were analyzed using R software with the DESeq2 package in Bioconductor. Subsequently, GSEA was performed using GSEA (version 3.0; Broad). The gene expression data were normalized with a log<sub>2</sub> fold change (FC > 1) along with an adjusted P-value (false discovery rate of ≤ 0.05), with the annotation information also provided.

## Statistical Analysis

Results are expressed as the mean ± standard deviation (SD). Differences between groups were evaluated by Student's t-test or one-way analysis of variance using GraphPad Prism 4 software. The log-rank Mantel-Cox test was used to compare Kaplan-Meier curves. In clinical cohort, categorical variables were described as frequencies, and differences were assessed using the chi-square test. Continuous variables are presented as medians with interquartile ranges, and differences were assessed using Wilcoxon rank-sum tests. The correlation between intracellular PKM2 expression and inflammatory biomarker levels was determined using Spearman's rank correlation. P values less than 0.05 were considered significant.

## SUPPLEMENTARY INFORMATION

The online version contains supplementary material available at <https://doi.org/10.1007/s10753-024-02000-x>.

## AUTHOR CONTRIBUTIONS

Shuangjun He, Yi Chen and Shuang Ye designed the study. Haiting Wang, Chenyu Fan, Xuelian Chen and Li Guo performed experiments and analyzed the data. Feng Zhao and Wei Zhou collected clinical samples. Haiting Wang, Shuangjun He and Chenyu Fan wrote the manuscript. All authors have read and approved the final manuscript.

## FUNDING

This work was supported by the National Natural Science Foundation of China (82172157).

## DATA AVAILABILITY

All data generated or analyzed during this study are included in this published article.

## DECLARATIONS

**Conflict of Interest** The authors declare no conflict of interest.

**OPEN ACCESS THIS ARTICLE IS LICENSED UNDER A CREATIVE COMMONS ATTRIBUTION 4.0 INTERNATIONAL LICENSE, WHICH PERMITS USE, SHARING, ADAPTATION, DISTRIBUTION AND REPRODUCTION IN ANY MEDIUM OR FORMAT, AS LONG AS YOU GIVE APPROPRIATE CREDIT TO THE ORIGINAL AUTHOR(S) AND THE SOURCE, PROVIDE A LINK TO THE CREATIVE COMMONS LICENCE, AND INDICATE IF CHANGES WERE MADE. THE IMAGES OR OTHER THIRD PARTY MATERIAL IN THIS ARTICLE ARE INCLUDED IN THE ARTICLE'S CREATIVE COMMONS LICENCE, UNLESS INDICATED OTHERWISE IN A CREDIT LINE TO THE MATERIAL. IF MATERIAL IS NOT INCLUDED IN THE ARTICLE'S CREATIVE COMMONS LICENCE AND YOUR INTENDED USE IS NOT PERMITTED BY STATUTORY REGULATION OR EXCEEDS THE PERMITTED USE, YOU WILL NEED TO OBTAIN PERMISSION DIRECTLY FROM THE COPYRIGHT HOLDER. TO VIEW A COPY OF THIS LICENCE, VISIT [HTTP://CREATIVECOMMONS.ORG/LICENSES/BY/4.0/](http://creativecommons.org/licenses/by/4.0/).**

## REFERENCES

1. Jose, R.J., and A. Manuel. 2020. COVID-19 cytokine storm: The interplay between inflammation and coagulation. *The Lancet Respiratory Medicine* 8: e46–e47.
2. Karki, R., B.R. Sharma, S. Tuladhar, et al. 2021. Synergism of TNF-alpha and IFN-gamma triggers inflammatory cell death, tissue damage, and mortality in SARS-CoV-2 infection and cytokine shock syndromes. *Cell* 184 (149–168): e117.
3. Mehta, P., D.F. McAuley, M. Brown, et al. 2020. COVID-19: Consider cytokine storm syndromes and immunosuppression. *Lancet* 395: 1033–1034.
4. Chousterman, B.G., F.K. Swirski, and G.F. Weber. 2017. Cytokine storm and sepsis disease pathogenesis. *Semin Immunopathol* 39: 517–528.
5. Behrens, E.M., S.W. Canina, K. Slade, et al. 2011. Repeated TLR9 stimulation results in macrophage activation syndrome-like disease in mice. *The Journal of Clinical Investigation* 121: 2264–2277.

## PKM2 Nuclear Translocation Regulate Ferroptosis-Associated ALI

- Wang, A., S.D. Pope, J.S. Weinstein, et al. 2019. Specific sequences of infectious challenge lead to secondary hemophagocytic lymphohistiocytosis-like disease in mice. *Proceedings of the National Academy of Sciences of the USA* 116: 2200–2209.
- Merad, M., and J.C. Martin. 2020. Pathological inflammation in patients with COVID-19: A key role for monocytes and macrophages. *Nature Reviews Immunology* 20: 355–362.
- Lucas, C., P. Wong, J. Klein, et al. 2020. Longitudinal analyses reveal immunological misfiring in severe COVID-19. *Nature* 584: 463–469.
- Huang, W., M. Li, G. Luo, et al. 2021. The inflammatory factors associated with disease severity to predict COVID-19 progression. *The Journal of Immunology* 206: 1597–1608.
- Qiu, P., X. Cui, J. Sun, et al. 2013. Antitumor necrosis factor therapy is associated with improved survival in clinical sepsis trials: A meta-analysis. *Critical Care Medicine* 41: 2419–2429.
- Li, J., F. Cao, H.L. Yin, et al. 2020. Ferroptosis: Past, present and future. *Cell Death & Disease* 11: 88.
- Mou, Y., J. Wang, J. Wu, et al. 2019. Ferroptosis, a new form of cell death: Opportunities and challenges in cancer. *Journal of Hematology & Oncology* 12: 34.
- Fang, X., H. Wang, D. Han, et al. 2019. Ferroptosis as a target for protection against cardiomyopathy. *Proceedings of the National Academy of Sciences of the USA* 116: 2672–2680.
- Zhu, H., A. Santo, Z. Jia, et al. 2019. GPx4 in bacterial infection and polymicrobial sepsis: Involvement of ferroptosis and pyroptosis. *React Oxy Species (Apex)* 7: 154–160.
- Tschopp, J., and K. Schroder. 2010. NLRP3 inflammasome activation: The convergence of multiple signalling pathways on ROS production? *Nature Reviews Immunology* 10: 210–215.
- Tadokoro, T., M. Ikeda, T. Ide, et al. 2020. Mitochondria-dependent ferroptosis plays a pivotal role in doxorubicin cardiotoxicity. *JCI Insight* 5(9): e132747.
- Gozzelino, R., and M.P. Soares. 2014. Coupling heme and iron metabolism via ferritin H chain. *Antioxidants & Redox Signaling* 20: 1754–1769.
- Zou, Y., W.S. Henry, E.L. Ricq, et al. 2020. Plasticity of ether lipids promotes ferroptosis susceptibility and evasion. *Nature* 585: 603–608.
- Gao, M., P. Monian, N. Quadri, et al. 2015. Glutaminolysis and transferrin regulate ferroptosis. *Molecular Cell* 59: 298–308.
- Lee, H., F. Zandkarimi, Y. Zhang, et al. 2020. Energy-stress-mediated AMPK activation inhibits ferroptosis. *Nature Cell Biology* 22: 225–234.
- Li, C., X. Dong, W. Du, et al. 2020. LKB1-AMPK axis negatively regulates ferroptosis by inhibiting fatty acid synthesis. *Signal Transduction and Targeted Therapy* 5: 187.
- Wang, X., S. Lu, C. He, et al. 2019. RSL3 induced autophagic death in glioma cells via causing glycolysis dysfunction. *Biochemical and Biophysical Research Communications* 518: 590–597.
- Palsson-McDermott, E.M., A.M. Curtis, G. Goel, et al. 2015. Pyruvate kinase M2 regulates Hif-1 $\alpha$  activity and IL-1 $\beta$  induction and is a critical determinant of the warburg effect in LPS-activated macrophages. *Cell Metabolism* 21: 65–80.
- Luo, W., H. Hu, R. Chang, et al. 2011. Pyruvate kinase M2 is a PHD3-stimulated coactivator for hypoxia-inducible factor 1. *Cell* 145: 732–744.
- Zhou, H.L., R. Zhang, P. Anand, et al. 2019. Metabolic reprogramming by the S-nitroso-CoA reductase system protects against kidney injury. *Nature* 565: 96–100.
- Shirai, T., R.R. Nazarewicz, B.B. Wallis, et al. 2016. The glycolytic enzyme PKM2 bridges metabolic and inflammatory dysfunction in coronary artery disease. *Journal of Experimental Medicine* 213: 337–354.
- Wang, H., P. An, E. Xie, et al. 2017. Characterization of ferroptosis in murine models of hemochromatosis. *Hepatology* 66: 449–465.
- Dixon, S.J., K.M. Lemberg, M.R. Lamprecht, et al. 2012. Ferroptosis: An iron-dependent form of nonapoptotic cell death. *Cell* 149: 1060–1072.
- Miotto, G., M. Rossetto, M.L. Di Paolo, et al. 2020. Insight into the mechanism of ferroptosis inhibition by ferrostatin-1. *Redox Biology* 28: 101328.
- Li, T., J. Han, L. Jia, et al. 2019. PKM2 coordinates glycolysis with mitochondrial fusion and oxidative phosphorylation. *Protein & Cell* 10: 583–594.
- Das Gupta, K., M.R. Shakespear, J.E.B. Curson, et al. 2020. Class IIa histone deacetylases drive toll-like receptor-inducible glycolysis and macrophage inflammatory responses via pyruvate kinase M2. *Cell Reports* 30 (2712–2728): e2718.
- Xie, M., Y. Yu, R. Kang, et al. 2016. PKM2-dependent glycolysis promotes NLRP3 and AIM2 inflammasome activation. *Nature Communications* 7: 13280.
- Evren, E., E. Ringqvist, K.P. Tripathi, et al. 2021. Distinct developmental pathways from blood monocytes generate human lung macrophage diversity. *Immunity* 54 (259–275): e257.
- Caricchio, R., M. Gallucci, C. Dass, et al. 2021. Preliminary predictive criteria for COVID-19 cytokine storm. *Annals of the Rheumatic Diseases* 80: 88–95.
- He, R., B. Liu, R. Xiong, et al. 2022. Itaconate inhibits ferroptosis of macrophage via Nrf2 pathways against sepsis-induced acute lung injury. *Cell Death Discovery* 8: 43.
- Yang, Y., Y. Wang, L. Guo, et al. 2022. Interaction between macrophages and ferroptosis. *Cell Death & Disease* 13: 355.
- Wang, Y., M. Zhang, R. Bi, et al. 2022. ACSL4 deficiency confers protection against ferroptosis-mediated acute kidney injury. *Redox Biology* 51: 102262.
- Liu, Z., Y. Le, H. Chen, et al. 2021. Role of PKM2-mediated immunometabolic reprogramming on development of cytokine storm. *Frontiers in Immunology* 12: 748573.
- Naidu, S.A.G., R.A. Clemens, and A.S. Naidu. 2023. SARS-CoV-2 infection dysregulates host iron (Fe)-redox homeostasis (Fe-R-H): Role of Fe-redox regulators, ferroptosis inhibitors, anticoagulants, and iron-chelators in COVID-19 control. *Journal of dietary supplements* 20: 312–371.
- Chen, D., Q. Zheng, L. Sun, et al. 2021. ORF3a of SARS-CoV-2 promotes lysosomal exocytosis-mediated viral egress. *Developmental Cell* 56 (3250–3263): e3255.
- Feng, Q., X. Yu, Y. Qiao, et al. 2022. Ferroptosis and acute kidney injury (AKI): Molecular mechanisms and therapeutic potentials. *Frontiers in Pharmacology* 13: 858676.
- Yin, X., G. Zhu, Q. Wang, et al. 2021. Ferroptosis, a new insight into acute lung injury. *Frontiers in Pharmacology* 12: 709538.
- Kung, Y.A., H.J. Chiang, M.L. Li, et al. 2022. Acyl-coenzyme a synthetase long-chain family member 4 is involved in viral replication organelle formation and facilitates virus replication via ferroptosis. *mBio* 13(1): e0271721.
- Bortolini, M., M.B. Wright, M. Bopst, et al. 2013. Examining the safety of PPAR agonists - current trends and future prospects. *Expert Opinion on Drug Safety* 12: 65–79.
- Sun, C., Y. Han, R. Zhang, et al. 2022. Regulated necrosis in COVID-19: A double-edged sword. *Frontiers in Immunology* 13: 917141.



46. Habib, H.M., S. Ibrahim, A. Zaim, et al. 2021. The role of iron in the pathogenesis of COVID-19 and possible treatment with lactoferrin and other iron chelators. *Biomedicine & Pharmacotherapy* 136: 111228.
47. Vlahakos, V.D., K.P. Marathias, N. Arkadopoulos, et al. 2021. Hyperferritinemia in patients with COVID-19: An opportunity for iron chelation? *Artificial Organs* 45: 163–167.
48. Markosyan, N., J. Li, Y.H. Sun, et al. 2019. Tumor cell-intrinsic EPHA2 suppresses anti-tumor immunity by regulating PTGS2 (COX-2). *The Journal of Clinical Investigation* 129: 3594–3609.
49. Kaur, B., and P. Singh. 2022. Inflammation: Biochemistry, cellular targets, anti-inflammatory agents and challenges with special emphasis on cyclooxygenase-2. *Bioorganic Chemistry* 121: 105663.
50. Michele, S., M.G. Salluzzo, A.E. Calogero, et al. 2014. Association study of COX-2 (PTGS2) -765 G/C promoter polymorphism by pyrosequencing in Sicilian patients with Alzheimer's disease. *Archives of Medical Science* 10: 1235–1238.
51. Xiao, X., Y. Jiang, W. Liang, et al. 2019. miR-212-5p attenuates ferroptotic neuronal death after traumatic brain injury by targeting Ptg2. *Molecular Brain* 12: 78.
52. Yang, W.S., R. SriRamaratnam, M.E. Welsch, et al. 2014. Regulation of ferroptotic cancer cell death by GPX4. *Cell* 156: 317–331.
53. Dang, G., T. Li, D. Yang, et al. 2022. T lymphocyte-derived extracellular vesicles aggravate abdominal aortic aneurysm by promoting macrophage lipid peroxidation and migration via pyruvate kinase muscle isozyme 2. *Redox Biology* 50: 102257.
54. Nandi, S., M. Razzaghi, D. Srivastava, et al. 2020. Structural basis for allosteric regulation of pyruvate kinase M2 by phosphorylation and acetylation. *Journal of Biological Chemistry* 295: 17425–17440.
55. Pucino, V., M. Certo, V. Bulusu, et al. 2019. Lactate buildup at the site of chronic inflammation promotes disease by inducing CD4(+) T cell metabolic rewiring. *Cell Metabolism* 30 (1055–1074): e1058.
56. Yang, W., Y. Xia, D. Hawke, et al. 2014. PKM2 phosphorylates histone H3 and promotes gene transcription and tumorigenesis. *Cell* 158: 1210.
57. Israelsen, W.J., and M.G. Vander Heiden. 2015. Pyruvate kinase: Function, regulation and role in cancer. *Seminars in Cell & Developmental Biology* 43: 43–51.
58. Jin, X., W. Zhang, Y. Wang, et al. 2020. Pyruvate kinase M2 promotes the activation of dendritic cells by enhancing IL-12p35 expression. *Cell Reports* 31: 107690.
59. Leu, J.I., M.E. Murphy, and D.L. George. 2020. Functional interplay among thiol-based redox signaling, metabolism, and ferroptosis unveiled by a genetic variant of TP53. *Proceedings of the National Academy of Sciences of the USA* 117: 26804–26811.
60. Yi, Z., Y. Wu, W. Zhang, et al. 2020. Activator-mediated pyruvate kinase M2 activation contributes to endotoxin tolerance by promoting mitochondrial biogenesis. *Frontiers in Immunology* 11: 595316.
61. Wu, Y., L. Ran, Y. Yang, et al. 2023. Deferasirox alleviates DSS-induced ulcerative colitis in mice by inhibiting ferroptosis and improving intestinal microbiota. *Life Sciences* 314: 121312.
62. Liu, Z., Y. Gu, A. Shin, et al. 2020. Analysis of myeloid cells in mouse tissues with flow cytometry. *STAR Protoc* 1: 100029.

**Publisher's Note** Springer Nature remains neutral with regard to jurisdictional claims in published maps and institutional affiliations.